BIOCHEMISTRY
including biophysical chemistry & molecular biology

Article

pubs.acs.org/biochemistry

Connection between Absorption Properties and Conformational Changes in *Deinococcus radiodurans* Phytochrome

Heikki Takala,[†,‡] Heli Lehtivuori,[†,§] Henrik Hammarén,[∥] Vesa P. Hytönen,[⊥,#] and Janne A. Ihalainen*[,†]

[†]Nanoscience Center, Department of Biological and Environmental Science, University of Jyväskylä, 40014 Jyväskylä, Finland
[‡]Department of Chemistry and Molecular Biology, University of Gothenburg, 40530 Gothenburg, Sweden
[§]Nanoscience Center, Department of Physics, University of Jyväskylä, 40014 Jyväskylä, Finland
[∥]School of Medicine, University of Tampere and Tampere University Hospital, 33520 Tampere, Finland
[⊥]BioMediTech, University of Tampere, 33520 Tampere, Finland
[#]Fimlab Laboratories, 33520 Tampere, Finland

Supporting Information

ABSTRACT: Phytochromes consist of several protein domains and a linear tetrapyrrole molecule, which interact as a red-light-sensing system. In this study, size-exclusion chromatography and light-scattering techniques are combined with UV−vis spectroscopy to investigate light-induced changes in dimeric *Deinococcus radiodurans* bacterial phytochrome (*Dr*BphP) and its subdomains. The photosensory unit (*Dr*CBD-PHY) shows an unusually stable Pfr state with minimal dark reversion, whereas the histidine kinase (HK) domain facilitates dark reversion to the resting state. Size-exclusion chromatography reveals that all phytochrome fragments remain as dimers in the illuminated state and dark state. Still, the elution profiles of all phytochrome fragments differ between the illuminated and dark states. The differences are observed reliably only when the whole UV−vis spectrum is characterized along the elution profile and show more Pfr-state characteristics at later elution volumes in *Dr*BphP and *Dr*CBD-PHY fragments. This implies that the PHY domain has an important role in amplifying and relaying light-induced conformational changes to the HK domain. In the illuminated state, the HK domain appears partially unfolded and prone to form oligomers. The oligomerization of *Dr*BphP can be diminished by converting the molecule back to the resting Pr state by using far-red light.

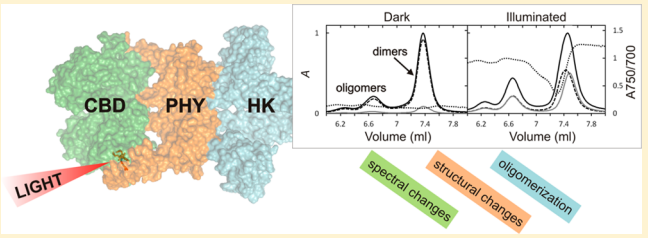

Phytochromes are light-sensing signaling proteins that control multiple key functions in plants and bacteria, including seed germination, flowering, and carotene production.[1,2] They are a family of dimeric photoreceptors sensitive to red and far-red light.[3−5] Red light causes canonical phytochrome to convert from a resting red-absorbing (Pr) state to an activated far-red-absorbing (Pfr) state, whereas far-red light or darkness reverts the protein back to the Pr state.[6] Canonical bacteriophytochromes (Figure 1D) consist of an N-terminal PAS (Per/Arndt/Sim) and GAF (cGMP phosphodiesterase/adenyl cyclase/FhlA) domain, which together form a chromophore-binding domain (CBD). CBD incorporates a linear tetrapyrrole biliverdin (BV) chromophore via a thioether linkage to a conserved cysteine (Cys24) residue.[3,7] CBD is connected to a phytochrome-associated (PHY) domain. Together the CBD and PHY domains constitute the photosensory region of the phytochrome, while the C-terminal signaling region of a bacteriophytochrome contains a histidine kinase (HK) domain, and the light-induced changes in photosensory region are relayed to the output region, HK domain, thus starting signaling events in cells.[8]

The structures of the dark (Pr) and illuminated (Pfr) states of bacterial phytochromes have received wide attention.[3,5,7,9,10] The crystal structures of several bacterial CBDs and photosensory regions have been solved in the dark resting state,[3,11,12] along with a cryoelectron microscope structure of the full-length bacteriophytochrome of *Deinococcus radiodurans*.[5] Structural information on the initial changes in the photocycle that occur close to the biliverdin chromophore has been obtained with crystallography and NMR,[9,13] as well as with temperature-scan cryocrystallography.[10] The structural changes in the rest of the phytochrome have, however, remained mostly speculative.

Structural studies on CBD fragments have revealed the most coherent picture of the initial structural changes in the bilin molecule. The incident red light leads to isomerization of the C15═C16 double bond between the C and D pyrrole rings of the BV.[14,15] The small light-induced changes in BV then initiate larger structural changes in the entire photosensory region. The crystal structures of the phytochrome photosensory regions show clear differences between Pr and Pfr states.[9,16] In particular, the crystal and solution structures of *Dr*CBD-PHY

Received: September 19, 2014
Revised: October 22, 2014
Published: October 22, 2014

   dx.doi.org/10.1021/bi501180s | *Biochemistry* 2014, 53, 7076−7085

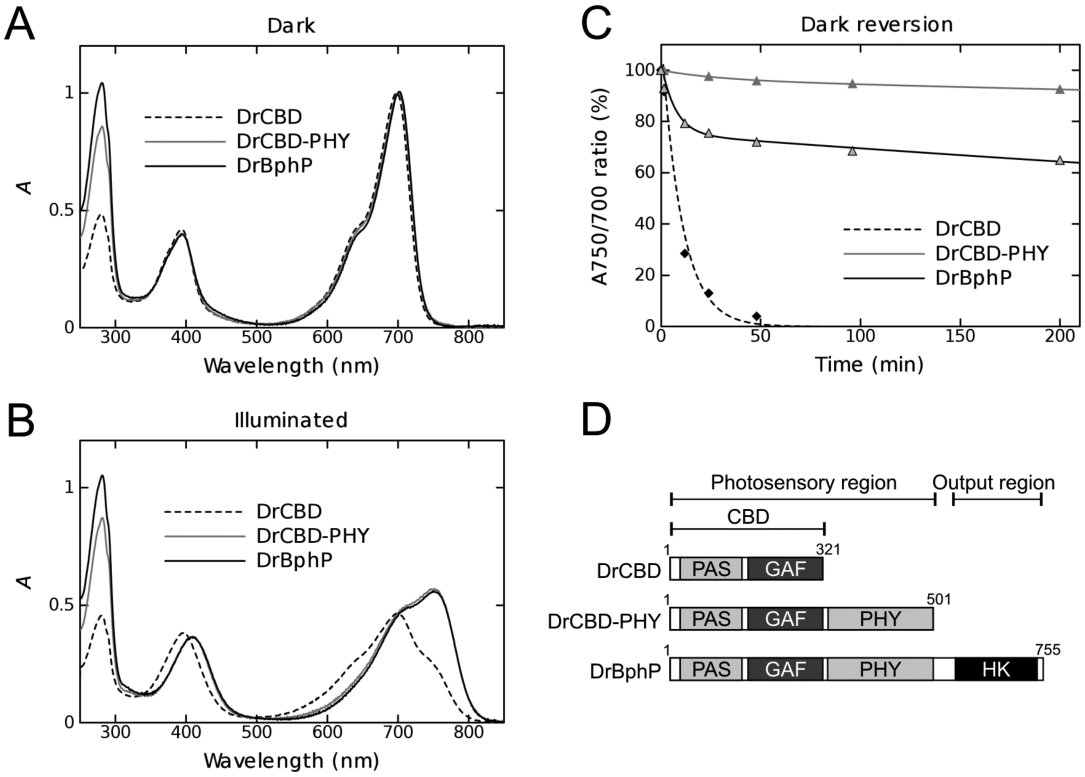

Figure 1. UV−vis absorption spectra of phytochrome constructs. Spectra measured (A) right after the sample was thawed (dark) and (B) after 15 min of 655 nm light illumination (illuminated). All absorption spectra were normalized using the dark sample as a reference at 700 nm (*Dr*CBD-PHY and *Dr*BphP) or at 698 nm (*Dr*CBD). (C) Dark reversion of each construct after illumination. The A_{750}/A_{700} ratio at each time point is determined by taking the ratio of the absorption signals at wavelengths of 750 and 700 nm. The graph is normalized such that 100% is the ratio after 15 min illumination, and 0% is the ratio of the initial dark state prior illumination. Solid lines show the exponential fits to the data. (D) Schematic representation of the *D. radiodurans* constructs used in this study.

in its dark and illuminated forms revealed the light-driven structural refolding of the PHY tongue extension in the vicinity of the BV molecule, which is followed by separation of long helices in the PHY domain.[16] Notable was, however, that the protein remained in the dimeric conformation, both in dark and in illuminated states.

The phytochromes from different species show variations in the angle between the GAF and PHY domains, which suggests flexibility in this area.[9] In addition, illumination-dependent monomer/dimer ratios of these complexes have been reported to vary between different species.[17−21] Biochemical assays such as limited proteolysis and size-exclusion chromatography, have hinted at the possibility of much more significant conformational flexibility in full-length phytochromes.[5,19,21] The cryo-EM study of full-length phytochrome has given information about the relative positions of HK and CBD-PHY domains in resting Pr state[5] and after illumination.[22] The light-induced repositioning of the HK domains of a phytochrome dimer, including the phosphoacceptor histidine residue relative to the ATP-binding site, has been proposed to cause HK domain activation.[5] It remains, however, a challenge to reveal the structural changes of soluble full-length phytochromes during a signal transduction event.

Here we have harnessed size-exclusion chromatography together with detailed UV−vis absorption and light-scattering analysis to study the light-induced chemical and conformational changes in *Deinococcus radiodurans* (*Dr*) phytochrome. The study reveals how each phytochrome domain experiences conformational changes during the photocycle and how this correlates to the absorption spectrum of the BV molecule. The direct connection between the quaternary organization of the phytochrome and the absorption properties of the BV chromophore is reported. Phytochrome fragments *Dr*CBD, *Dr*CBD-PHY, and full-length *Dr*BphP (Figure 1D) were used to show how these conformational changes are reflected in the size distribution, hydrodynamic properties, and quaternary assemblies of the protein.

MATERIALS AND METHODS

Expression Vectors. The expression constructs, coding domains *Dr*CBD (residues 1−321) and *Dr*CBD-PHY (residues 1−502) and a full-length *Deinococcus radiodurans* phytochrome (residues 1−755), were kindly provided by the laboratories of Prof. R. D. Vierstra and Prof. K. T. Forest.[7] The *Dr*CBD, *Dr*CBD-PHY, and full-length *Dr*BphP coding sequences were in the pET21b(+) vector containing a C-terminal His6-tag (Novagen). The vector coding *Synechocystis* PCC6803 hemeoxygenase (Ho1) is described elsewhere.[23]

Protein Expression and Purification. The constructs were coexpressed in *Escherichia coli* strain BL21 (DE3) (Novagen) with Ho1 and purified as described in refs 16 and 23. *Dr*CBD-PHY was expressed without Ho1. To encourage full BV loading to the protein, the cleared cell lysate was incubated on ice overnight with at least 10× molar excess of BV (Frontier Scientific). The protein was purified with an ÄKTA Prime instrument utilizing Ni-NTA affinity chromatography (HisTrap, GE Healthcare) followed by Superdex 200 size-exclusion chromatography (GE Healthcare) in final buffer of 20

dx.doi.org/10.1021/bi501180s | *Biochemistry* 2014, 53, 7076−7085

mM Tris, 150 mM NaCl, pH 7.0. In the case of the *Dr*BphP construct, only fractions containing the dimeric product were selected. All purification steps were conducted in the dark. Purified protein was concentrated to 20−40 mg/mL, flash-frozen, and stored at −80 °C.

Sample Illumination Conditions. To obtain the "dark" sample, the phytochrome constructs were used right after thawing or irradiated with a far-red LED light (780 nm with output power of 9 mW corresponding a photon flux of about 750 μmol m^{-2} s^{-1}) for 15 min. The dark-adapted samples and the samples after far-red illumination were fully comparable. The use of far-red light in the experiment is reported separately. For the "illuminated" sample, the phytochromes were irradiated with a red LED light (655 nm with output power of 7 mW corresponding a photon flux of about 490 μmol m^{-2} s^{-1}) for 15 min before each measurement. Illumination was performed in ambient conditions, and in each case it was controlled so that the photoequilibrium was reached. Unless otherwise indicated, the samples were kept in the dark before and during the experiments.

UV−Vis Spectroscopy. The UV−vis spectra were measured with the PerkinElmer LAMBDA 850 UV−vis spectrophotometer. The samples were diluted with buffer (20 mM Tris, 150 mM NaCl, pH 7.0) to obtain OD_{280} close to 0.1.

Size-Exclusion Chromatography (SEC) with Multi-wavelength Detection and Online Light-Scattering Analysis. The size-exclusion measurements were conducted with Yarra 3u SEC-3000 (300 mm × 7.80 mm) columns (Phenomenex, Torrance, US) and a mobile phase of 20 mM Tris, 150 mM NaCl, pH 7.0. Prior to SEC analysis, protein samples were illuminated in 5−6 mg/mL concentration until photoequilibrium was established, and 30 μg was injected for each chromatographic run.

For SEC with multiwavelength UV−vis detection, the samples were analyzed using the Shimadzu HPLC VP10 pumping system (Shimadzu Corporation, Kyoto, Japan). The elution fractions were analyzed with a diode array UV−vis detector (SPD-M10A, Shimadzu Corporation). The detection rate was reported to be 1.5625 Hz, yielding data points in approximately 0.01 min resolution. Experiments were executed with 1 mL/min flow-rate in ambient conditions, and each analysis was repeated three to four times. The repeats yielded highly reproducible retention times (Figure S1, Supporting Information), where average deviations between the runs were 0.01−0.03 min. The protein size marker standard (Phenomenex) was used according to the manufacturer's instructions. The molecular weights of the phytochrome fragments were determined by calculating a standard curve of the molecular weight marker proteins myoglobin (17 kDa), ovalbumin (44 kDa), IgG (150 kDa), IgA (300 kDa), and bovine thyroglobulin (670 kDa), shown in Figure S2, Supporting Information. The void volume in Yarra 3u SEC-300 is reported to be 5.5−5.6 min (5.54 and 5.62; 1 mL/min flow rate).

For SEC with online light scattering analysis (SEC-SLS), the samples were analyzed using a liquid chromatography instrument (CBM-20A, Shimadzu Corporation, Kyoto, Japan) equipped with an autosampler (SIL-20A), UV−vis (SPD-20A), and Zetasizer μV SLS/DLS detector (Malvern Instruments Ltd., Worcestershire, U.K.) to determine the molecular weight and size. The instrument was controlled using Lab Solutions, version 5.51 (Shimadzu Corporation) and OmniSEC 4.7 (Malvern). The runs were executed with a flow rate of 0.4 mL/min at +20 °C. The molecular weight was determined according to the elution time by calculating a standard curve of the molecular weight marker (Bio-Rad) proteins myoglobulin (17 kDa), ovalbumin (44 kDa), γ-globulin (158 kDa), and thyroglobulin (670 kDa). In addition, the molecular mass was determined based on the light-scattering intensity of the eluting protein, for which the instrument was calibrated using the monomeric fraction of BSA as a standard in OmniSEC software (Malvern Instruments Ltd.). The use of BSA as a standard for light scattering was validated separately.

Dynamic Light Scattering (DLS). Dynamic light scattering was conducted using a Malvern Zetasizer μV instrument (Malvern Instruments Ltd.) with a 90° detection angle and a laser wavelength of 830 nm. The laser wavelength was chosen to interfere minimally with the phytochrome photocycle. The DLS measurements of *Dr*CBD-PHY and *Dr*BphP were conducted in 30 mM Tris, pH 8.0, at +20 °C. Each protein was analyzed by performing 15 measurements each consisting of 10 × 10 s data collection runs. The molecular weight of the protein was estimated from the hydrodynamic radius using a globular protein standard curve from the manufacturer.

Limited Proteolysis and Mass Analysis. Limited proteolysis using chymotrypsin was conducted in 20 mM Tris, 150 mM NaCl, pH 7.0, in the presence of the 1:1000 ratio of α-chymotrypsin (Sigma) as described in ref 24. All incubations were conducted at room temperature. Fractions containing bound BV were detected with zinc-induced fluorescence[25] in which the SDS-PAGE gel was treated with 10 mM zinc acetate prior UV detection.

For mass spectroscopy analysis of *Dr*CBD-PHY and *Dr*BphP, the proteolysis was stopped with 0.2% trifluoroacetic acid (TFA), and 2 or 5 μL of sample was injected to a LCMS system (UPLC with a Waters BEH300 C4 column, 2.1 mm × 100 mm). Proteins were eluted with a 15 min gradient from 3/97% ACN/water to 70/30% ACN/water containing 0.2% formic acid. Detection was done with a Synapt G2 Q-Tof mass spectrometer (Waters) operated with electrospray ionization in positive mode. Spectra were deconvoluted with MaxEnt 1 for larger proteins or MaxEnt 3 for isotopically resolved peptides (10 kDa or smaller). Experimental masses were identified against the phytochrome construct sequence with FindPept tool of the ExPASy Server.[26] All cysteines were reduced in the calculations. The theoretical monomeric molecular masses were calculated from protein sequence by using the ProtParam tool.[27] The molar mass of biliverdin was estimated to be 582.6 g/mol.

RESULTS

UV−Vis Analysis Reveals Distinct Spectral Properties of Constructs. The UV−vis spectra of the three phytochrome constructs (*Dr*CBD, *Dr*CBD-PHY, and *Dr*BphP, illustrated in Figure 1D) before and after illumination with 655 nm light are shown in Figure 1A,B. In the dark state, all three constructs show very similar absorption spectra on the BV region, at 350−800 nm, which is in line with results reported by other groups (e.g., see refs 28 and 29). The spectra are normalized to the maximum at 700 nm of the dark state and, thus, show different absorption values at the 280 nm aromatic amino acid band, illustrating the different aromatic residue/BV ratios. After illumination, the absorption band at around 700 nm of BV (Figure 1A), called the *Q*-band, shifts toward red in all samples (Figure 1B). In the case of *Dr*CBD-PHY and *Dr*BphP, the *Q*-band spectra show typical Pfr state spectra resembling earlier results from other studies.[29,30] *Dr*CBD yields a different

dx.doi.org/10.1021/bi501180s | *Biochemistry* 2014, 53, 7076−7085

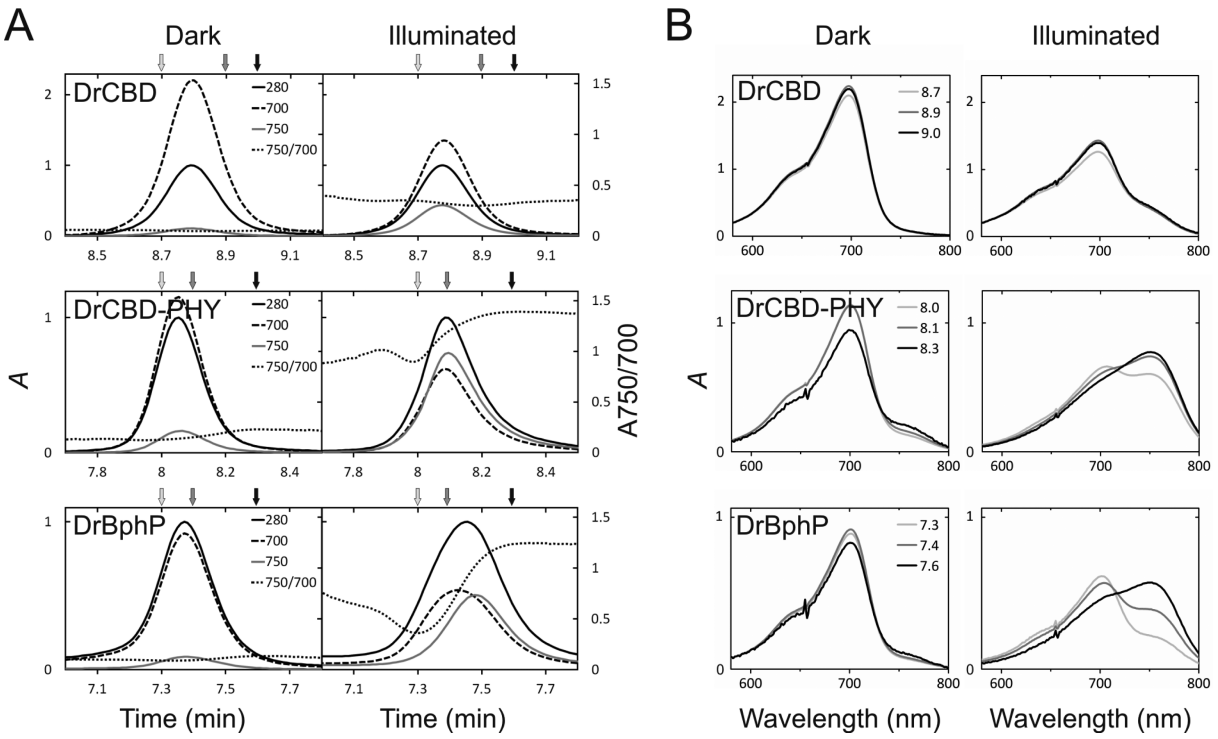

Figure 2. Size-exclusion chromatography (SEC) analysis of phytochrome constructs. (A) The elution profile of the phytochrome constructs after 780 nm illumination (dark) and after 655 nm illumination (illuminated). The elution profile is plotted in three wavelengths (280, 700, and 750 nm) in order to visualize the changes in absorption and retention. Elution graphs are normalized to the maximum of each 280 nm plot. The absorbance ratio (A_{750}/A_{700}) is plotted in the same panels, and their values are plotted to the right *y*-axis of the graph. (B) The absorption spectra of the phytochrome Q-bands at selected retention times, after 780 nm illumination (dark) or after 655 nm illumination (illuminated), marked as arrows in panel A.

illuminated spectrum compared with the *Dr*CBD-PHY and *Dr*BphP samples (Figure 1B), implying an incomplete or a different type of photocycle.[20,21,28,29] It is also notable that the absorption band at around 400 nm, a so-called Soret band, is different in the illuminated *Dr*CBD sample compared with the *Dr*CBD-PHY and *Dr*BphP samples. Further on in this study, the ratio of wavelengths 750 and 700 nm (A_{750}/A_{700}) is used as a sample-specific indication of the relative amounts of the photoproducts of the phytochrome samples. In the illuminated form, the *Dr*CBD has an A_{750}/A_{700} ratio of 0.54, while that of the *Dr*CBD-PHY and *Dr*BphP is 1.22.

The dark reversion kinetics of the constructs was measured by detecting spectra sequentially after 655 nm illumination. The reversion rates of the samples varied markedly between the constructs (Figure 1C). The *Dr*CBD constructs returned to the Pr state most rapidly, whereas the *Dr*CBD-PHY and the *Dr*BphP constructs required substantially more time. The dark reversion of *Dr*CBD-PHY was strikingly slow compared with other phytochrome fragments, indicating an extremely stable Pfr state for this fragment. To obtain a time constant for the dark reversion, the data was fitted with exponential functions, as in refs 21 and 31. This procedure revealed a monoexponential return time of about 10 min for *Dr*CBD (RMSE = 0.0324). Implementing a second time constant for a multiexponential function, with time values of 9 and 117 min, improved the fit only marginally (0.0316). However, monoexponential fits appeared unsatisfactory in the case of *Dr*CBD-PHY (0.0097) and *Dr*BphP (0.0890), and clearly better fit was obtained by using a sum of two time constants (RMSE = 0.0015 and 0.0148, respectively). The time constants obtained from the biexponential fits were 29 min (with decay amplitude of 4%) and 4991 min (96%) for *Dr*CBD-PHY and 7 min (24%) and 1291 min (76%) for *Dr*BphP. The DrBphP data follows the observations by Wagner et al., which qualitatively also imply a biexponential dark reversion rate.[29] Similar observations have been obtained in studies with plant (*Secale cereale* cv Balbo) and *Agrobacterium tumefaciens* (Agp1) phytochrome systems.[21,31] In these studies, two time constants for dark reversion have been observed: a fast component similar to the one presented here but faster rates for the slow component (350 min for plant and 160 min for Agp1 phytochrome).

Photoconverted States Elute Differently in Size-Exclusion Chromatography. The changes in the UV−vis spectra of the phytochrome fragments tell of structural and chemical changes only in the vicinity of the BV molecule. We therefore continued to investigate whether these changes in absorption are accompanied by light-induced changes in other measures in the rest of the phytochrome molecule. To accomplish this, diode-array-detected UV−vis spectra in combination with size-exclusion chromatography (SEC) were studied. This allowed us to study changes in protein size and shape and correlate them to changes in the UV−vis absorption properties of the sample. Figure 2A shows the protein retention at three wavelengths, which enables simultaneous inspection of overall protein retention (λ = 280 nm), elution of mainly Pr-state proteins (λ = 700 nm), and elution of mainly Pfr-state proteins (λ = 750 nm). The absorption ratio (A_{750}/A_{700}) was plotted to reflect the relative amount of Pfr state proteins compared with Pr state. In addition, the Q-band spectra of three selected retention times from each run (arrows in Figure 2A) were plotted to directly visualize the photoactive state of the fragment (Figure 2B).

dx.doi.org/10.1021/bi501180s | *Biochemistry* 2014, 53, 7076−7085

Table 1. Apparent Molecular Sizes Detected with Protein Hydrodynamics of the Dark Samples

	DLS			SEC−UV−vis		SEC−SLS		
	R_h (nm)	PdI	MW (kDa)[a]	t (min)	MW (kDa)	t (min)	MW/SEC (kDa)	MW/LS (kDa)
DrCBD				8.8	58			
DrCBD-PHY	4.5 ± 0.8	0.22	110 ± 20	8.0	119	9.1	105	126
DrBphP	6.2 ± 1.1	0.31	240 ± 50	7.4	227	8.2	240	290

[a]Molecular weight indicated from DLS are estimates based on a globular protein model.

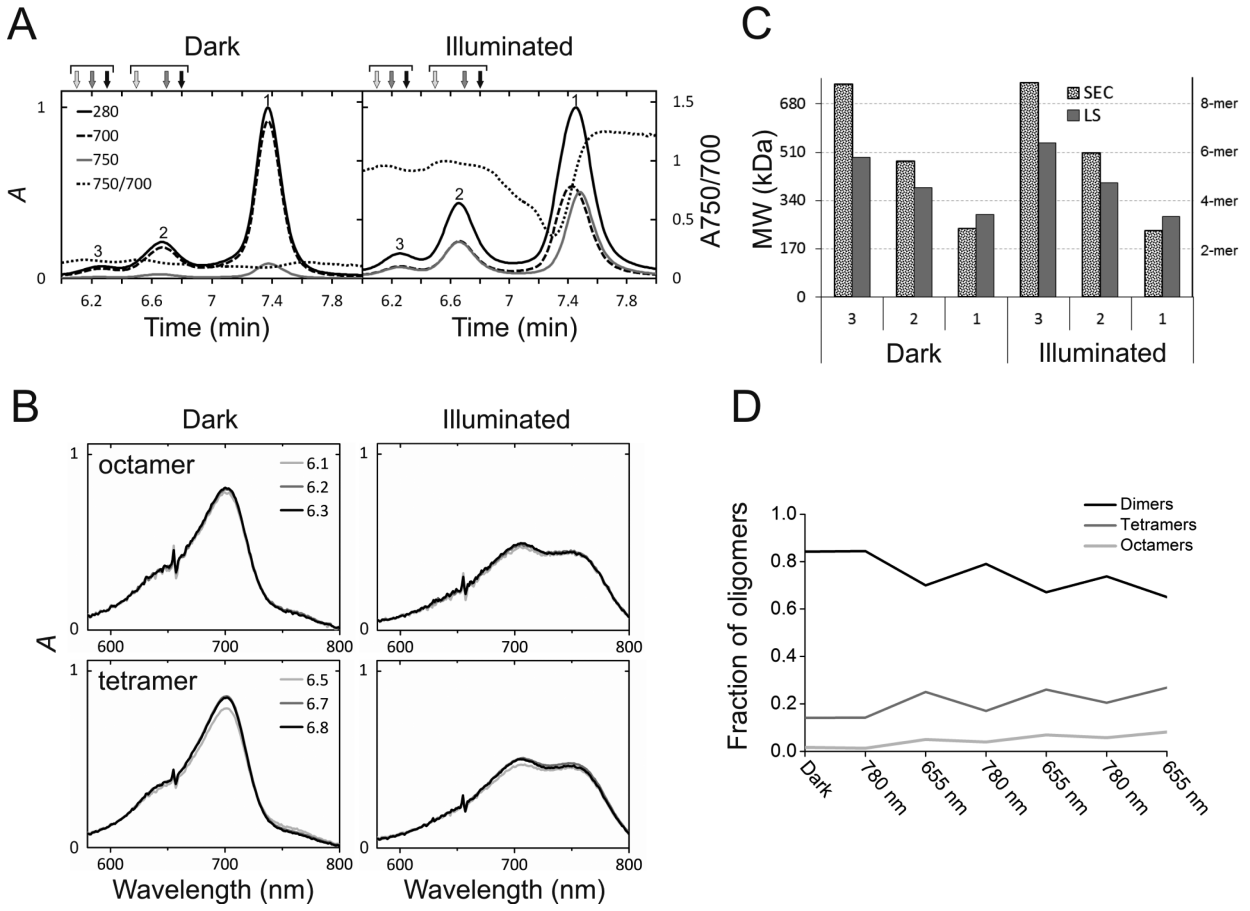

Figure 3. Light-induced oligomerization of *Dr*BphP. (A) The elution profiles of full-length *Dr*BphP after 780 nm illumination (dark) and after 655 nm illumination (illuminated). The elution profiles are plotted in three wavelengths (280, 700, and 750 nm) and are normalized to the maximum of each 280 nm plot. The absorbance ratio (A_{750}/A_{700}) is plotted in the same panels, and the values are plotted to the right y-axis of the graph. (B) Absorption spectra of the phytochrome Q-bands at the selected retention times corresponding to tetramers and octamers, after 780 nm illumination (dark) or after 655 nm illumination (illuminated), marked in as arrows in panel A. (C) Molecular weight estimates of *Dr*BphP oligomer peaks calculated from the elution time (SEC) and right-angle light scattering (LS). The peak numbers are indicated in panel A. (D) Relative fractions of various oligomeric species during the cycle between the Pr and Pfr states. Each elution graph is plotted at A_{280nm} and normalized to the area under the curve (i.e., to the amount of protein injected). Light-driven oligomerization is partially reversible, but the total trend of net oligomerization is present.

The dark sample of *Dr*CBD (Figure 2, top panels) eluted as a single peak with homogeneous Pr absorption spectra along the whole elution time. Only small heterogeneity, which is indicated as an almost linear A_{750}/A_{700} ratio plot, in the absorption spectra along the elution time was observed (Figure 2A, dotted line). In addition, selected elution times exhibited almost identical spectra resembling Pr state (Figure 2B). The A_{280} retention time, 8.8 min, implies a dimeric *Dr*CBD construct of 58 kDa globular size (Table 1; predicted, 74.4 kDa). After red light illumination, the mobility of the sample shifted slightly to lower retention times. The average A_{750}/A_{700} ratio (0.33) was smaller than in batch UV−vis measurements (0.54, see above), in line with rapid dark reversion of *Dr*CBD to the Pr state (Figure 1C) during the SEC run.

Dark *Dr*CBD-PHY sample (Figure 2, middle panels) eluted as a single peak with a time of 8.0 min, indicating a dimeric protein size of 119 kDa (Table 1). This is comparable to the dimer size calculated from sequence (113 kDa). Illumination shifted the average mobility of the protein to a higher retention time and broadened the chromatogram toward higher retention times. The UV−vis absorption spectra of the dark sample appeared fairly homogeneous with absorption spectra resembling the Pr state. More importantly, the UV−vis spectra of the illuminated sample varied considerably along the retention peak (Figure 2B, middle panel). The nonlinear A_{750}/A_{700} ratio plot

dx.doi.org/10.1021/bi501180s | *Biochemistry* 2014, 53, 7076−7085

of the sample had a minimum at 8.0 min and a maximum at 8.3 min, indicating that molecules with the highest 750 nm absorption, that is, the most Pfr-like spectra, eluted later than molecules with Pr-like spectra. The maximum value of the A_{750}/A_{700} ratio (1.39) was higher than that obtained from batch UV−vis measurements (1.22, see above). The average A_{750}/A_{700} ratio of the entire elution plot (1.18) was, however, similar to the batch UV−vis measurements (1.22). This is in line with the minimal, 5%, dark reversion of the *Dr*CBD-PHY construct (Figure 1C).

The majority of the dark full-length *Dr*BphP (Figure 2, bottom panels; Table 1) eluted in a peak with a maximum at 7.4 min. The retention time indicates a dimer of 227 kDa size (Table 1), which is larger than predicted from the amino acid sequence (168 kDa). The full *Dr*BphP elution plot with oligomeric peaks is shown in Figure 3A and discussed later. The dimeric fraction behaved in a way resembling *Dr*CBD-PHY: The illumination shifted the retention maxima to higher retention times, and broadened the peaks. The shift is even larger than in the case of *Dr*CBD-PHY. The UV−vis absorption spectra of the dark sample were again homogeneous, whereas clear spectral heterogeneity along the elution peak, even more pronounced than in the case of *Dr*CBD-PHY, was present in the illuminated sample (Figure 2B, bottom panels). The highly nonlinear A_{750}/A_{700} ratio plot had a minimum at 7.3 min and a maximum at 7.6 min. This indicates that molecules with lowest absorption at 750 nm, closely resembling the Pr state, eluted in the first half of the peak and the molecules with strongest 750 nm absorption eluted significantly later (Figure 2B, bottom panels), indicating a retention-dependent enrichment of Pfr state molecules. The maximum value of the A_{750}/A_{700} ratio (1.25) was similar to that obtained from batch UV−vis measurements (1.22, see above). However, the averaged A_{750}/A_{700} ratio of the dimeric part (0.91) is lower than expected from the dark-reverted batch UV−vis data (80% reverted after 12 min, Figure 1C), which can be explained by slow dark reversion of the oligomeric species obtained with *Dr*BphP samples (*vide infra*).

DLS Reveals Mainly Dimeric Nature of the Samples. Utilizing batch DLS technique, the size of the particles can be determined in terms of hydrodynamic radius in a matrix-free experiment. In line with the HPLC−SEC measurement, batch DLS data verified the dimeric nature of the *Dr*CBD-PHY and *Dr*BphP proteins (Table 1). The attained hydrodynamic radii were converted to molecular sizes assuming a globular molecular shape of the dark state molecules (Table 1). The batch DLS measurements did not detect significant light-induced changes in the hydrodynamic radius of *Dr*CBD-PHY (data not shown), confirming its dimeric nature during the photocycle. The measurements with full-length *Dr*BphP, on the other hand, revealed a light-induced increase in hydrodynamic radius, which was a result of light-induced oligomerization (*vide infra;* see also Figure 3A).

To obtain information about the molecular mass of the particle eluted in SEC, light-scattering data (SLS) was measured during SEC separation. The scattering profiles were constant within the elution peaks both in the dark and in the illuminated samples (data not shown). This suggests the existence of identical oligomeric states throughout each elution peak.

Light-Dependent Oligomerization of Full-Length *Dr*BphP. Size-exclusion measurements of the full-length *Dr*BphP construct resulted in additional elution peaks corresponding to larger oligomers (Figures 3A and 4). According to the relative elution times and the light-scattering

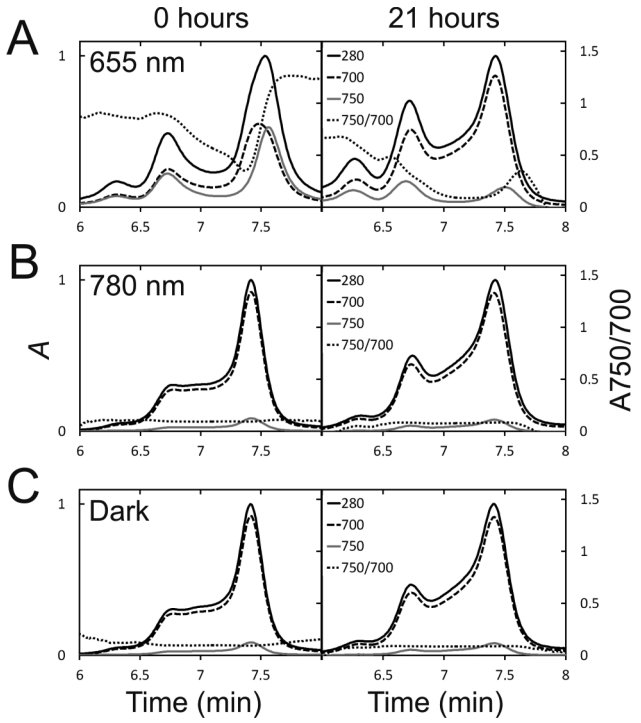

Figure 4. Dark reversion of the *Dr*BphP oligomers. Three identical *Dr*BphP samples were (A) illuminated 15 min with 655 nm light, (B) illuminated with 780 nm light, or (C) kept in the dark. The samples were analyzed with SEC immediately after illumination (left panels, 0 h) and after 21 h of dark incubation (right panels, 21 h). The elution profiles are plotted in three wavelengths (280, 700, and 750 nm) and are normalized to the maximum of each 280 nm plot. The absorbance ratio (A_{750}/A_{700}) is plotted in the same panels, and the values are plotted to the right *y*-axis of the graph. All experiments were conducted at room temperature.

signals, these peaks appeared as tetramers and hexamers and octamers (Figure 3C). The mobility of the tetrameric and octametric fractions changed marginally after illumination to lower retention times. In contrast to the dimeric fraction (Figure 2B), the larger oligomers are spectrally very homogeneous (Figure 3B); that is, their absorption spectrum does not vary notably as a function of retention time. The dark oligomers appear as Pr state molecules whereas the illuminated spectra appear as partial Pfr with relatively low 750 nm absorption (Figure 3B) when compared with the dimeric species (Figure 2B). This homogeneity is also seen in the A_{750}/A_{700} ratio plot (Figure 3A, dotted line), in which the values (in the range 0.8−1.0) do not vary notably along the dimeric peak.

The oligomer content in full-length *Dr*BphP can be robustly controlled with red and far-red light. *Dr*BphP formed larger oligomers after 655 nm light illumination, that is, in the Pfr state. However, after reversion of the dimers and oligomers back to the Pr state with far-red light, the oligomerization was reduced. This can be seen with sequential illumination with red (655 nm) and far-red (780 nm) light before the sample injections to the HPLC (Figure 3D), which reveals a trend with an increasing number of larger oligomers at the expense of dimers. The deoligomerization was only partial, although all the particles returned to the Pr state (Figure 3C).

dx.doi.org/10.1021/bi501180s | *Biochemistry* 2014, 53, 7076−7085

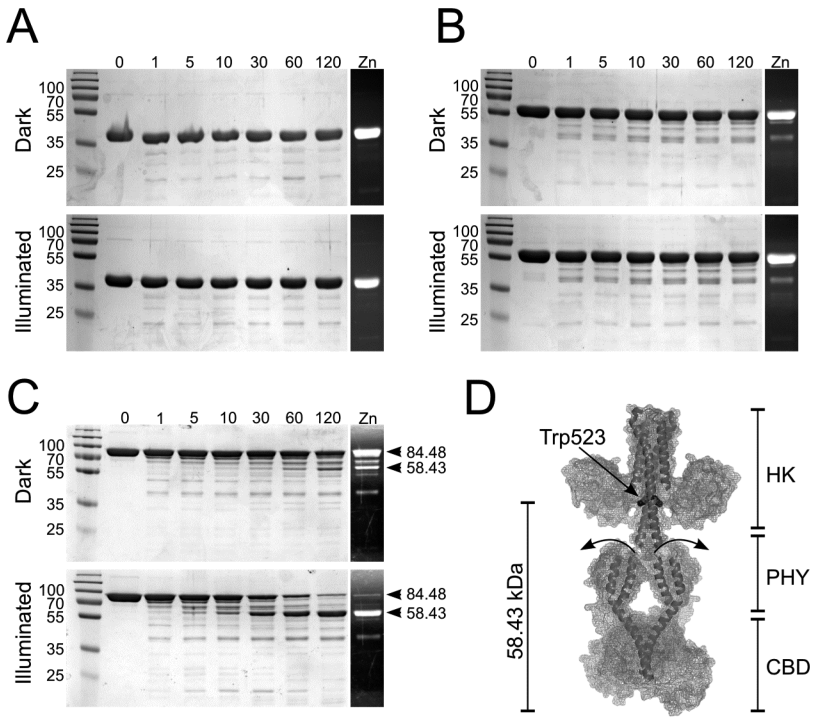

Figure 5. Limited proteolysis of phytochrome constructs. Proteolysis of (A) *Dr*CBD, (B) *Dr*CBD-PHY, and (C) *Dr*BphP was conducted either in the dark (dark) or under constant 655 nm illumination (illuminated). The time points of the SDS-PAGE samples taken during the proteolysis are indicated at the top of the gels (in minutes). The molecular masses of the marker proteins are on the left-hand side of the gels. The gels on the left are stained for protein; the gel fragments on the right (Zn) are labeled using zinc-induced fluorescence[25] to reveal bound biliverdin. The zinc-labeled gel fragment corresponds to the last (120 min) time point of the gel. (D) Proposed model of the full-length *Dr*BphP in Pr with Trp523 where the light-induced proteolysis occurs is marked. For the model, DrCBD-PHY in Pr (PBD code 4O0P)[16] and a structure of *Thermotoga maritima* sensor histidine kinase (PDB code 2c2a)[33] were used like in Yang et al. 2008.[12] The opening of the *Dr*CBD-PHY dimer[16] is indicated as curved arrows.

Oligomerization of *Dr*BphP Restricts Dark Reversion. The full-length *Dr*BphP was shown to oligomerize in the Pfr state. Next, the long-term oligomerization and its effects on the dark reversion were studied. This was achieved by comparing the elution profiles and the spectral signatures of the dark and illuminated samples after long-term dark incubation (Figure 4). If the sample was illuminated with far-red light (Figure 4B) or kept in the dark (Figure 4C) relatively little oligomerization occurred; if the sample was left in the dark after red light illumination, it continued to oligomerize (Figure 4A). The A_{750}/A_{700} ratio in the SEC chromatogram indicated normal reversion to Pr state in the dimeric fraction whereas the higher oligomeric states remained mostly in the Pfr state (Figure 4A, 21 h). The A_{750}/A_{700} ratio remained higher at lower retention times. In addition to illumination, the presence of ions affected oligomerization: the SEC and DLS experiments revealed that excluding NaCl from the buffer prevented the oligomerization process, which is consistent with a previous study with a plant phytochrome.[32] Small pH changes near neutral value (7.0−8.0) did not affect the oligomerization.

Limited Proteolysis of the Phytochrome Constructs. We have shown with SEC in combination with UV−vis detection how light-induced conformational changes are relayed to the HK domain via the PHY domain. Limited proteolysis was applied to study how these changes affect the solvent accessibility of each protein domain (Figure 5). Each construct was treated with chymotrypsin either in the dark state or under constant 655 nm illumination. *Dr*CBD and *Dr*CBD-PHY appeared resistant to proteolysis (Figure 5A), and the red light illumination did not affect their susceptibility for degradation. Mass spectrometry analysis of *Dr*CBD-PHY fragment after proteolysis yielded a single peak of 56.97 kDa, which corresponds to the full *Dr*CBD-PHY construct without its first methionine in the N-terminal T7 tag (calculated mass from sequence 56972.7 g/mol).

In contrast to *Dr*CBD and *Dr*CBD-PHY, the full-length *Dr*BphP (84.48 kDa from mass spectrometry analysis) showed little susceptibility to proteolysis in its dark state (Figure 5C). Interestingly, *Dr*BphP degradation was notably increased by red light (655 nm) illumination. The illuminated sample was more readily degraded than the dark sample. The resulting proteolytic fragment was 58.43 kDa in size and contained BV according to the zinc-induced fluorescence.[25] Mass analysis against the construct sequence revealed that the resulting fragment includes the N-terminal T7 tag from the cloning vector (MASMTGGQQMGRGS) without its first methionine and the phytochrome residues 1−523 (58431.4 g/mol). The site susceptible to the proteolysis, next to Trp523, can be predicted to locate in the long dimerization helix that extends from the PHY domain to the HK domain (Figure 5D).[12] This assumption is based on the homologous histidine kinase structure of *Thermotoga maritima* sensor histidine kinase (PDB code 2c2a)[33] and on the assumption that the long dimerization helix is continuous between PHY and HK domain.

■ DISCUSSION

Understanding the light-induced changes in phytochromes requires structural data on atomic detail as well as understanding their biochemical behavior in the buffer environment. In this study, a relationship between changes in the size-related

dx.doi.org/10.1021/bi501180s | *Biochemistry* 2014, 53, 7076−7085

properties of phytochrome and its chromophore spectrum has been pointed out for three fragments, consisting of a chromophore-binding domain (*Dr*CBD), a photosensory core region (*Dr*CBD-PHY), and the full-length *Dr*BphP including a histidine kinase domain (*Dr*CBD-PHY-HK).

Dark Reversion Is Facilitated by HK. *Dr*CBD shows an impaired photocycle and monoexponential dark reversion that was clearly faster than that of longer fragments (Figure 1). *Dr*CBD-PHY and *Dr*BphP, which reach the Pfr state, show slower and multiexponential dark reversion. The results are consistent with previous measurements with *Dr*BphP[22,29] and very similar to those obtained for plant and Agp1 phytochromes that also include two decay components.[21,31] Rather surprisingly, the *Dr*CBD-PHY exhibits a considerably slower dark reversion rate (Figure 1C). Such a stable photoactivated state, which is easily switched back by far-red illumination, is clearly beneficial to further applications and biophysical characterization of the *Dr*CBD-PHY fragment. This impaired dark reversion, for example, allowed the crystallization of the photosensory unit in the illuminated state.[16] Furthermore, it could enable its utilization as a more stable optogenetic switch. The very slow reversion is in contrast to the faster dark reversion of *Agrobacterium* photosensory region (Agp1-M15).[21] In addition, our observations with *Dr*CBD deviate slightly from those of the Agp1 counterpart (Agp1-M20), which shows monoexponential reversion with a time constant comparable to the larger constructs.[21] The HK domain facilitates the dark reversion of *Dr*BphP. However, the HK domain resides far from the BV in the phytochrome molecule and interacts only indirectly with the chromophore.[5] Our structural studies showed that the long dimerization helices of the PHY domain appear far apart in the illuminated state.[16] In an intuitive picture, the helices need to approach each other during the dark reversion. This is an unlikely event in *Dr*CBD-PHY, but plausible in the full-length *Dr*BphP where the HK restricts the conformational space and therefore facilitates the dark reversion.

Light-Induced Changes in Size and Solvent Accessibility. Our data report links between UV−vis absorption and size-exclusion elution properties of three *D. radiodurans* fragments. The *Dr*CBD-PHY and *Dr*BphP fragments behaved similarly in the size-exclusion experiments (Figure 2): The complexes with highest 750 nm (Pfr) absorption eluted slower than the ones with higher 700 nm (Pr) absorption. However, the exact Pr and Pfr composition of the phytochrome dimers at each elution point remain unresolved with the method. *Dr*CBD retention was less affected by illumination. The large light-induced change in the retention of longer fragments confirms the role of the PHY domain in relaying and amplifying the initial conformational changes caused by illumination.[16] The results also suggest that this change is further amplified in the HK domain.

The slower retention of Pfr state proteins could suggest more compact structures in the Pfr state than in the Pr state. The structures of *Dr*CBD-PHY in its dark and illuminated forms[16] indicate, however, a larger steric exclusion radius in the illuminated form than in the dark form. The CBD-PHY crystal structures from other species in the resting state[11,12,16] also adopt a compact conformation. The illuminated state therefore cannot be more compact than the dark state. The alternative reasons for the difference in retention lie either in (1) the subunit organization, implying variations in dimer stability, or (2) conformational changes that cause changes in SEC-retention in ways different than suggested above. These potential ways include changes in the penetration of the pores in the SEC column or interactions with the column matrix. Attempts to determine the light-dependent changes in the hydrodynamic size of the *Dr*CBD-PHY molecules with DLS did not reveal notable changes. According to Wang et al. such a hydrodynamic size parameter would be the best description for interpretation of the SEC elution profiles,[34] but this unfortunately does not apply in this case. Thus, other parameters such as particle shape or hydrophobic interactions are likely to play a role in the elution profiles.

Similar SEC experiments have been conducted with *Synechococystis*[18] and *Agrobacterium* phytochromes,[21] as well as some plant phytochromes.[17] In those studies, the illuminated state appeared larger than the resting state, which has been explained by light-induced changes in dimerization. Studies with full-length Agp1 did not show a mobility difference between states, whereas the Agp1-M15 (CBD-PHY) fragment appeared larger in the Pfr state.[21] In the case of Cph1, a CBD-PHY fragment (called F1) was shown to monomerize in Pr state,[19] which implies a behavior resembling Agp1-M15. Interestingly, monomerized full-length Cph1 fragments behaved in SEC in a way closely resembling the *Dr*CBD-PHY presented here. Still, the structural changes inside a CBD-PHY monomer can be universal to canonical phytochromes.[16] Illumination causes the bending of the long scaffolding helix, which leads to changes in the dimerization stability. The differences between the phytochromes from various species could therefore be a result of different dimer stability and protein monomerization. In this study, *Dr*BphP remains dimeric, and the results are not affected by monomerization. This is also supported by structural data presented elsewhere: *Dr*BphP has a stable dimerization interface between CBDs and a second interface between HK domains.[3,5,16,22] Further investigation is needed to explain how the light-induced changes are reflected in size-exclusion elution.

The limited proteolysis (Figure 5) reveals that the Pfr state of *Dr*BphP undergoes structural changes that expose or partially unfold regions after the PHY domain. The unfolding exposes Trp523 in the predicted dimerization and histidine phosphotransfer (DHp) subdomains of the HK domain, which shares a long scaffolding helix with the PHY domain (Figure 5D). These results are consistent with previous studies with an artificial restriction site in *Dr*BphP[5,35] and closely resemble the results obtained with full-length Agp1[21] and Cph1.[19] As the *Dr*CBD-PHY dimer opens up in response to red light illumination[16] (arrows in Figure 5D), the HK domains of the phytochrome dimer may experience rotation, reorganization, or detachment from each other. *Dr*CBD-PHY proteolysis remains insensitive to the illumination, which actually contrasts the observations with of Cph1 F1 and the Agp1-M15 fragments where differences between the Pr and Pfr susceptibility were reported.[19,21] This discrepancy implies that the light-induced structural changes that lead to different solvent accessibility in CBD-PHY fragments vary between the species.

Light-Controllable Oligomerization of Phytochromes. Combining SEC and LS (Figure 3) showed that full-length *Dr*BphP oligomerizes in a light-induced manner. Pea (*Pisum sativa*) phytochrome has been briefly reported to oligomerize after red light illumination,[36] and other plant phytochromes form oligomers in a solvent-dependent manner.[37−39] Because smaller phytochrome fragments (*Dr*CBD and *Dr*CBD-PHY) did not show the oligomerization effect, it must be driven by

dx.doi.org/10.1021/bi501180s | *Biochemistry* 2014, 53, 7076−7085

the HK domain. A partial unfolding of the HK domain in the Pfr state can increase its susceptibility for proteolysis and its solvent accessibility, which then leads to oligomerization. Oligomerization takes place at physiological NaCl concentrations (150 mM) and is greatly diminished by excluding NaCl from the solvent. This phenomenon might be linked to NaCl-induced differences in the solubility or stability of the protein, but the details of the process are unknown.

The spectral characteristics of the larger oligomers differ from dimeric species. The illuminated oligomers absorb less at 750 nm compared with illuminated dimers (Figures 2B and 3B). This can be due to different pigment−protein interaction in the vicinity of the BV molecule[40] or a lower population of Pfr state molecules. The dark reversion of the larger oligomers is also notably slower than that of the dimeric part (Figure 4). Indeed, dark reversion in a plant phytochrome is shown to be hindered by excess interacting proteins.[41] Nuclear bodies in *Arabidopsis thaliana* are shown to serve as storage sites of phytochrome B (phyB) and to protect Pfr state from dark reversion by stabilizing the Pfr-state molecules.[42] The *Dr*BphP dimers in the Pfr state form complexes *in vitro* where the phytochrome molecules interact with each other. These interactions then obstruct normal dark reversion. This same steric hindrance may be one cause of the formation of incomplete Pfr spectra in the oligomers (see Figure 3B, illuminated).

Optogenetics is a field of research where cell behavior is modulated by light (for example, refs 43−45). It has recently gained wide attention among photosensor researchers. Light-controlled oligomerization of *Arabidopsis thaliana* cryptochrome 2, for example, has led to an application where cellular signaling pathways are remodeled using blue light.[46] *Dr*BphP oligomerized preferably in its Pfr state (Figure 5), which enables one-way control of phytochrome oligomerization by illumination. Phytochromes offer a great advantage over blue-light sensors: better penetration of red light used for phytochromes allows deeper tissues and thicker sample layers to be studied.[47] In this study, we detected light-dependent oligomerization in the physiological NaCl concentration and at close to neutral pH. In cells, oligomerization could facilitate the function of signaling protein by creating specific signaling complexes.[48] The oligomerization studies here were conducted *in vitro* and with relatively high protein concentrations. Further studies will show whether this occurs also *in vivo*.

To conclude, this study reveals conformational changes that phytochrome constructs from *Deinococcus radiodurans* undergo when switching between Pr and Pfr states. The changes in size and shape that each phytochrome domain undergoes are linked to the chromophore spectra. These light-induced changes are relayed to the HK domain, changing its solvent accessibility. The results further our understanding of the structural changes in phytochromes. They accompany the work done with *Dr*CBD-PHY, which explained the light-induced structural changes within the photosensory core module,[16] and they set the basis for further studies with full-length *Dr*BphP.

■ ASSOCIATED CONTENT

Supporting Information

Resolution and reproducibility of the SEC experiments and Size-exclusion of molecular weight standard mixture. This material is available free of charge via the Internet at http://pubs.acs.org.

■ AUTHOR INFORMATION

Corresponding Author

*Tel: (+358) 400-247979. E-mail: janne.ihalainen@jyu.fi.

Funding

This work was supported by Finnish Academy Grants 138063 (J.A.I., H.L., and H.T.) and 136288 (V.P.H.) and by the Finnish Cultural Foundation Grant (J.A.I. and 0131067 H.T.).

Notes

The authors declare no competing financial interest.

■ ACKNOWLEDGMENTS

We thank Alli Liukkonen, Ilona Rissanen, and Lauri Nuuttila for the assistance in laboratory work. We acknowledge Ulrich Bergmann for help in mass spectroscopy. We also thank Biocenter Finland and The Council of Tampere region for infrastructure support.

■ ABBREVIATIONS

BV, biliverdin; CBD, chromophore-binding domain; DLS, dynamic light scattering; HK, histidine kinase; HPLC, high-performance liquid chromatography; PHY, phytochrome-associated domain; SEC, size-exclusion chromatography

■ REFERENCES

(1) Davis, S. J., Vener, A. V., and Vierstra, R. D. (1999) Bacteriophytochromes: Phytochrome-like photoreceptors from non-photosynthetic eubacteria. *Science 286*, 2517−2520.

(2) Quail, P. H. (2002) Phytochrome photosensory signalling networks. *Nat. Rev. Mol. Cell Biol. 3*, 85−93.

(3) Wagner, J. R., Brunzelle, J. S., Forest, K. T., and Vierstra, R. D. (2005) A light-sensing knot revealed by the structure of the chromophore-binding domain of phytochrome. *Nature 438*, 325−331.

(4) Rockwell, N. C., Su, Y. S., and Lagarias, J. C. (2006) Phytochrome structure and signaling mechanisms. *Annu. Rev. Plant Biol. 57*, 837−858.

(5) Li, H., Zhang, J., Vierstra, R. D., and Li, H. (2010) Quaternary organization of a phytochrome dimer as revealed by cryoelectron microscopy. *Proc. Natl. Acad. Sci. U. S. A. 107*, 10872−10877.

(6) Eilfeld, P., and Rüdiger, W. (1985) Absorption spectra of phytochrome intermediates. *Z. Naturforsch., C: J. Biosci. 40c*, 109−114.

(7) Wagner, J. R., Zhang, J., Brunzelle, J. S., Vierstra, R. D., and Forest, K. T. (2007) High resolution structure of deinococcus bacteriophytochrome yields new insights into phytochrome architecture and evolution. *J. Biol. Chem. 282*, 12298−12309.

(8) Ulijasz, A. T., and Vierstra, R. D. (2011) Phytochrome structure and photochemistry: Recent advances toward a complete molecular picture. *Curr. Opin. Plant Biol. 14*, 498−506.

(9) Yang, X., Kuk, J., and Moffat, K. (2009) Conformational differences between the pfr and pr states in pseudomonas aeruginosa bacteriophytochrome. *Proc. Natl. Acad. Sci. U. S. A. 106*, 15639−15644.

(10) Yang, X., Ren, Z., Kuk, J., and Moffat, K. (2011) Temperature-scan cryocrystallography reveals reaction intermediates in bacteriophytochrome. *Nature 479*, 428−432.

(11) Essen, L. O., Mailliet, J., and Hughes, J. (2008) The structure of a complete phytochrome sensory module in the pr ground state. *Proc. Natl. Acad. Sci. U. S. A. 105*, 14709−14714.

(12) Yang, X., Kuk, J., and Moffat, K. (2008) Crystal structure of *Pseudomonas aeruginosa* bacteriophytochrome: Photoconversion and signal transduction. *Proc. Natl. Acad. Sci. U. S. A. 105*, 14715−14720.

(13) Ulijasz, A. T., Cornilescu, G., Cornilescu, C. C., Zhang, J., Rivera, M., Markley, J. L., and Vierstra, R. D. (2010) Structural basis for the photoconversion of a phytochrome to the activated pfr form. *Nature 463*, 250−254.

(14) Mroginski, M. A., Murgida, D. H., and Hildebrandt, P. (2007) The chromophore structural changes during the photocycle of

phytochrome: A combined resonance raman and quantum chemical approach. *Acc. Chem. Res. 40*, 258−266.
(15) Rockwell, N. C., Shang, L., Martin, S. S., and Lagarias, J. C. (2009) Distinct classes of red/far-red photochemistry within the phytochrome superfamily. *Proc. Natl. Acad. Sci. U. S. A. 106*, 6123−6127.
(16) Takala, H., Bjorling, A., Berntsson, O., Lehtivuori, H., Niebling, S., Hoernke, M., Kosheleva, I., Henning, R., Menzel, A., Ihalainen, J. A., and Westenhoff, S. (2014) Signal amplification and transduction in phytochrome photosensors. *Nature 509*, 245−248.
(17) Lagarias, J. C., and Mercurio, F. M. (1985) Structure function studies on phytochrome. Identification of light-induced conformational changes in 124-kDa avena phytochrome in vitro. *J. Biol. Chem. 260*, 2415−2423.
(18) Lamparter, T., Esteban, B., and Hughes, J. (2001) Phytochrome Cph1 from the cyanobacterium synechocystis PCC6803. Purification, assembly, and quaternary structure. *Eur. J. Biochem. 268*, 4720−4730.
(19) Esteban, B., Carrascal, M., Abian, J., and Lamparter, T. (2005) Light-induced conformational changes of cyanobacterial phytochrome Cph1 probed by limited proteolysis and autophosphorylation. *Biochemistry 44*, 450−461.
(20) Noack, S., and Lamparter, T. (2007) Light modulation of histidine-kinase activity in bacterial phytochromes monitored by size exclusion chromatography, crosslinking, and limited proteolysis. *Methods Enzymol. 423*, 203−221.
(21) Noack, S., Michael, N., Rosen, R., and Lamparter, T. (2007) Protein conformational changes of agrobacterium phytochrome Agp1 during chromophore assembly and photoconversion. *Biochemistry 46*, 4164−4176.
(22) Burgie, E. S., Wang, T., Bussell, A. N., Walker, J. M., Li, H., and Vierstra, R. D. (2014) Crystallographic and electron microscopic analyses of a bacterial phytochrome reveal local and global rearrangements during photoconversion. *J. Biol. Chem. 289*, 24573−24587.
(23) Lehtivuori, H., Rissanen, I., Takala, H., Bamford, J., Tkachenko, N. V., and Ihalainen, J. A. (2013) Fluorescence properties of the chromophore-binding domain of bacteriophytochrome from *Deinococcus radiodurans*. *J. Phys. Chem. B 117*, 11049−11057.
(24) Takala, H., and Ylanne, J. (2012) Binding properties and stability of the ras-association domain of Rap1-GTP interacting adapter molecule (RIAM). *PLoS One 7*, No. e31955.
(25) Berkelman, T. R., and Lagarias, J. C. (1986) Visualization of bilin-linked peptides and proteins in polyacrylamide gels. *Anal. Biochem. 156*, 194−201.
(26) Gattiker, A., Bienvenut, W. V., Bairoch, A., and Gasteiger, E. (2002) FindPept, a tool to identify unmatched masses in peptide mass fingerprinting protein identification. *Proteomics 2*, 1435−1444.
(27) Wilkins, M. R., Gasteiger, E., Bairoch, A., Sanchez, J. C., Williams, K. L., Appel, R. D., and Hochstrasser, D. F. (1999) Protein identification and analysis tools in the ExPASy server. *Methods Mol. Biol. 112*, 531−552.
(28) Auldridge, M. E., Satyshur, K. A., Anstrom, D. M., and Forest, K. T. (2012) Structure-guided engineering enhances a phytochrome-based infrared fluorescent protein. *J. Biol. Chem. 287*, 7000−7009.
(29) Wagner, J. R., Zhang, J., von Stetten, D., Gunther, M., Murgida, D. H., Mroginski, M. A., Walker, J. M., Forest, K. T., Hildebrandt, P., and Vierstra, R. D. (2008) Mutational analysis of *Deinococcus radiodurans* bacteriophytochrome reveals key amino acids necessary for the photochromicity and proton exchange cycle of phytochromes. *J. Biol. Chem. 283*, 12212−12226.
(30) Bhoo, S. H., Davis, S. J., Walker, J., Karniol, B., and Vierstra, R. D. (2001) Bacteriophytochromes are photochromic histidine kinases using a biliverdin chromophore. *Nature 414*, 776−779.
(31) Correll, D. L., Edwards, J. L., and Shropshire, W., Jr. (1968) Multiple chromophore species in phytochrome. *Photochem. Photobiol. 8*, 465−475.
(32) Sarkar, H. K., Moon, D. K., Song, P. S., Chang, T., and Yu, H. (1984) Tertiary structure of phytochrome probed by quasi-elastic light scattering and rotational relaxation time measurements. *Biochemistry 23*, 1882−1888.
(33) Marina, A., Waldburger, C. D., and Hendrickson, W. A. (2005) Structure of the entire cytoplasmic portion of a sensor histidine-kinase protein. *EMBO J. 24*, 4247−4259.
(34) Wang, Y., Teraoka, I., Hansen, F. Y., Peters, G. H., and Hassager, O. (2010) A theoretical study of the separation principle in size exclusion chromatography. *Macromolecules 43*, 1651−1659.
(35) Yoon, J. M., Hahn, T. R., Cho, M. H., Jeon, J. S., Bhoo, S. H., and Kwon, Y. K. (2008) The PHY domain is required for conformational stability and spectral integrity of the bacteriophytochrome from *Deinococcus radiodurans*. *Biochem. Biophys. Res. Commun. 369*, 1120−1124.
(36) Nakasako, M., Iwata, T., Inoue, K., and Tokutomi, S. (2005) Light-induced global structural changes in phytochrome A regulating photomorphogenesis in plants. *FEBS J. 272*, 603−612.
(37) Pratt, L. H. (1973) Comparative immunochemistry of phytochrome. *Plant Physiol. 51*, 203−209.
(38) Grombein, S., and Rudiger, W. (1976) On the molecular weight of phytochrome: A new high molecular phytochrome species in oat seedlings. *Hoppe-Seyler's Z. Physiol. Chem. 357*, 1015−1018.
(39) Boeshore, M. L., and Pratt, L. H. (1980) Phytochrome modification and light-enhanced, in vivo-induced phytochrome pelletability. *Plant Physiol. 66*, 500−504.
(40) Nieder, J. B., Stojkovic, E. A., Moffat, K., Forest, K. T., Lamparter, T., Bittl, R., and Kennis, J. T. (2013) Pigment-protein interactions in phytochromes probed by fluorescence line narrowing spectroscopy. *J. Phys. Chem. B 117*, 14940−14950.
(41) Sweere, U., Eichenberg, K., Lohrmann, J., Mira-Rodado, V., Baurle, I., Kudla, J., Nagy, F., Schafer, E., and Harter, K. (2001) Interaction of the response regulator ARR4 with phytochrome B in modulating red light signaling. *Science 294*, 1108−1111.
(42) Rausenberger, J., Hussong, A., Kircher, S., Kirchenbauer, D., Timmer, J., Nagy, F., Schafer, E., and Fleck, C. (2010) An integrative model for phytochrome B mediated photomorphogenesis: From protein dynamics to physiology. *PLoS One 5*, No. e10721.
(43) Deisseroth, K. (2011) Optogenetics. *Nat. Methods 8*, 26−29.
(44) Levskaya, A., Weiner, O. D., Lim, W. A., and Voigt, C. A. (2009) Spatiotemporal control of cell signalling using a light-switchable protein interaction. *Nature 461*, 997−1001.
(45) Christie, J. M., Gawthorne, J., Young, G., Fraser, N. J., and Roe, A. J. (2012) LOV to BLUF: Flavoprotein contributions to the optogenetic toolkit. *Mol. Plant 5*, 533−544.
(46) Bugaj, L. J., Choksi, A. T., Mesuda, C. K., Kane, R. S., and Schaffer, D. V. (2013) Optogenetic protein clustering and signaling activation in mammalian cells. *Nat. Methods 10*, 249−252.
(47) Shu, X., Royant, A., Lin, M. Z., Aguilera, T. A., Lev-Ram, V., Steinbach, P. A., and Tsien, R. Y. (2009) Mammalian expression of infrared fluorescent proteins engineered from a bacterial phytochrome. *Science 324*, 804−807.
(48) Cebecauer, M., Spitaler, M., Serge, A., and Magee, A. I. (2010) Signalling complexes and clusters: Functional advantages and methodological hurdles. *J. Cell Sci. 123*, 309−320.